



Aalborg Universitet

AALBORG UNIVERSITY  
DENMARK

## An Online Parameters Monitoring Method for Output Capacitor of Buck Converter Based on Large-Signal Load Transient Trajectory Analysis

Zhao, Zhaoyang; Lu, Weiguo; Davari, Pooya; Du, Xiong; Ho-Ching lu, Herbert ; Blaabjerg, Frede

*Published in:*

I E E E Journal of Emerging and Selected Topics in Power Electronics

*DOI (link to publication from Publisher):*

[10.1109/JESTPE.2020.2964068](https://doi.org/10.1109/JESTPE.2020.2964068)

*Publication date:*

2021

*Document Version*

Accepted author manuscript, peer reviewed version

[Link to publication from Aalborg University](#)

*Citation for published version (APA):*

Zhao, Z., Lu, W., Davari, P., Du, X., Ho-Ching lu, H., & Blaabjerg, F. (2021). An Online Parameters Monitoring Method for Output Capacitor of Buck Converter Based on Large-Signal Load Transient Trajectory Analysis. *I E E E Journal of Emerging and Selected Topics in Power Electronics*, 9(4), 4004 - 4015. Article 8950189. <https://doi.org/10.1109/JESTPE.2020.2964068>

### General rights

Copyright and moral rights for the publications made accessible in the public portal are retained by the authors and/or other copyright owners and it is a condition of accessing publications that users recognise and abide by the legal requirements associated with these rights.

- Users may download and print one copy of any publication from the public portal for the purpose of private study or research.
- You may not further distribute the material or use it for any profit-making activity or commercial gain
- You may freely distribute the URL identifying the publication in the public portal -

### Take down policy

If you believe that this document breaches copyright please contact us at [vbn@aub.aau.dk](mailto:vbn@aub.aau.dk) providing details, and we will remove access to the work immediately and investigate your claim.

# An Online Parameters Monitoring Method for Output Capacitor of Buck Converter Based on Large-Signal Load Transient Trajectory Analysis

Zhaoyang Zhao, Weiguo Lu, *Member, IEEE*, Pooya Davari, *Senior Member, IEEE*, Xiong Du, *Member, IEEE*, Herbert Ho-Ching Iu, *Senior Member, IEEE*, and Frede Blaabjerg, *Fellow, IEEE*

**Abstract**—Aluminum Electrolytic Capacitor (AEC) is one of the weakest components in power electronic converters. As the degradation of AEC happens, its equivalent series resistance (*ESR*) increases and the capacitance (*C*) decreases. Therefore, online monitoring of *ESR* and *C* to predict AEC's life has great significance for ensuring safe and reliable operation of converters. In this paper, an online monitoring scheme is proposed for buck converters, aiming to estimate the *ESR* and *C* of AEC at the output side. The proposed scheme utilizes large-signal load transient trajectories to estimate the AEC parameters and has a relatively low sampling frequency. By analyzing the relationship between the transient trajectory and capacitor parameters, the *ESR* is directly calculated using the voltage and current step values at the initial instant of the transient. Further, *C* is calculated utilizing a calculation model derived from the output-voltage load transient trajectory. Corresponding simulation analysis and an online monitoring system implementation are provided. Furthermore, a 48V-12V buck converter with a digital PI controller and an analog  $V^2$  controller is built to verify the proposed online estimation method. The experimental results of the estimated *ESR* and *C* are consistent with the results measured by an LCR meter, and the estimation error is less than 10%.

**Index Terms**—Aluminum electrolytic capacitor (AEC), online monitoring, equivalent series resistance (*ESR*), capacitance (*C*), large-signal load transient trajectory.

## I. INTRODUCTION

Aluminum electrolytic capacitors (AEC) is one of the key components in power electronic converters [1]–[3], but it is vulnerable to degradation and causes converter failures [4]–[6]. As reported in [7] and [8] around 30% of the faults in converters are due to the aging of AECs. So it is essential to

monitor the health state of AEC and replace it with a healthy one before its degradation [9]–[11].

Recent studies have illustrated that the equivalent series resistance (*ESR*) of AEC increases and the capacitance (*C*) decreases with the degradation of the AEC [12]. Generally, the AEC is considered to have lapsed when the *ESR* increases to 2.8 times and/or the *C* reduces to 80% of its initial value at the same temperature [13]. Therefore, various *ESR* and *C* monitoring methods are proposed to assess the health state of AEC in dc-dc converters. In [14]–[16], offline approaches including sinusoidal waveforms injection method and physical assessment method are proposed to obtain the *ESR* and *C*. These methods are easily implemented, however, they impact the normal operation of the converter [17].

To improve the drawback of offline methods, different *ESR* and/or *C* online monitoring approaches are introduced for dc-dc converters in [18]–[41]. One commonly used *ESR* and *C* online monitoring method is small-perturbation-injection (SPI) based method. In [18], a low-frequency small perturbation signal is injected to the duty cycle and the health of the AEC is estimated using the low-frequency impedance. In [19]–[22], a pseudo-random binary sequence (PRBS) is injected to the duty cycle, then the parameters of the converter are obtained based on the average model. These methods have realized the full parameters monitoring of the dc-dc converter. However, a large amount of time is required to run complex identification algorithms. The switching frequency of the above-mentioned converters is relatively low (20 kHz), which limit their application in high-frequency dc-dc converters. Moreover, the perturbation signals may easily impose additional power losses in the converters.

As the steady-state ripple signals of dc-dc converters are directly related to the capacitor parameters, various steady-state ripple (SSR) based methods are proposed to reduce the complexity of identification algorithms. In [23], the *ESR* of a buck converter is estimated based on the dc value of capacitor voltage ripple extracted using filter and rectifier circuits. In [24], the ripple voltage jump and the inductor current peak are sampled to obtain the *ESR* of a boost converter. In [25]–[29], the *ESR* is calculated based on the relationship between ripple voltage and inductor current. These methods mentioned above effectively estimate the *ESR* of AEC in dc-dc converters. However, special-designed current sensors, oscilloscope, PC,

Manuscript received October 28, 2019; revised December 16, 2019; accepted December 30, 2019. This work was supported by the National Key Research and Development Program of China under Grant 2018YFB0905803. (Corresponding author: Weiguo Lu and Pooya Davari).

Z. Zhao, W. Lu and X. Du are with the State Key Laboratory of Power Transmission Equipment & System Security and New Technology, Chongqing University, Chongqing 400044, China (e-mail: zhaoyang.z@foxmail.com; luweiguo@cqu.edu.cn; duxiong@cqu.edu.cn).

H. H.-C. Iu is with the School of Electrical, Electronics and Computer Engineering, University of Western Australia, Crawley, WA 6009, Australia (e-mail: herbert.iu@uwa.edu.au).

P. Davari and F. Blaabjerg are with the Department of Energy Technology, Aalborg University, Aalborg 9220, Denmark (e-mail: pda@et.aau.dk; fbl@et.aau.dk).

and/or high-speed data acquisition card are required to extract and analyze the high-frequency small-amplitude ripple signals [30]. Considering the film capacitor across AEC may reduce the estimation accuracy of  $ESR$ , it is essential to add the monitoring of  $C$ . [2] and [31] use the voltage ripple sampled at particular instants to calculate the  $ESR$  and  $C$  of the AEC. This method can online estimate both  $ESR$  and  $C$ . And, the implementation is relatively simple, but the amplification factor of the ripple extraction circuit cannot be adaptive to the temperature variation, which decreases the estimation accuracy [32]. Moreover, various circuit model (CM) based methods are proposed to online estimate AEC parameters [33]–[39]. The estimation accuracy of these methods is relatively high, however, they require high-speed sampling devices to accurately obtain the circuit parameters (the sampling frequency is more than 150 times the switching frequency of converters), which increases the hardware cost.

To avoid the sampling of high-frequency small-amplitude ripple signals, an output voltage transient analysis based scheme is proposed for a full-bridge converter in [40]. The implementation of the online estimation of  $ESR$  is easy, but it does not provide an accurate estimation model and the error is relatively large. Moreover, using the data fitting of transient voltage, a capacitance estimation scheme is proposed for a phase-shifted ZVS converter in [41]. However, it is a quasi-online monitoring scheme. As we know, non-isolated buck converters often encounter step change in the load current, which causes an output voltage deviation during transients [42]. Compared with the high-frequency small-amplitude steady-state ripple signals, the transient voltage deviation has the features of large-amplitude and long time scale. By analyzing the relationship between the large-signal load transient trajectory and capacitor parameters, this paper presents an online monitoring scheme for buck converters, aiming to estimate the output capacitor's  $ESR$  and  $C$ . The  $ESR$  is directly calculated using the voltage and current step values at the initial instant of the transient. The  $C$  is calculated utilizing the calculation model derived from the output voltage transient trajectory. Experimental results demonstrate that the proposed online  $ESR$  and  $C$  estimation method is feasible.

This paper is organized as follows: Section II presents the idea of the proposed AEC online estimation scheme. Section III gives the calculation model of  $ESR$  and  $C$  as well as the simulation results. Section IV describes the implementation method and experimental results. Finally, conclusions are drawn in Section V.

## II. THE PROPOSED MONITORING SCHEME

In this paper, a large-signal transient trajectory analysis (LS-TTA) based scheme is proposed to online estimate the aluminum electrolytic capacitors (AEC) parameters of a buck converter. Referring to Fig. 1, the buck converter is comprised of two individual semiconductor switches  $S_1$  (indicated in purple),  $S_2$  (indicated in blue), output inductor  $L$ , and output capacitor  $C_o$ , where the output capacitor (AEC) is equivalent to

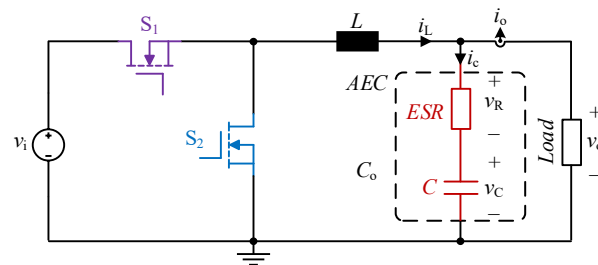
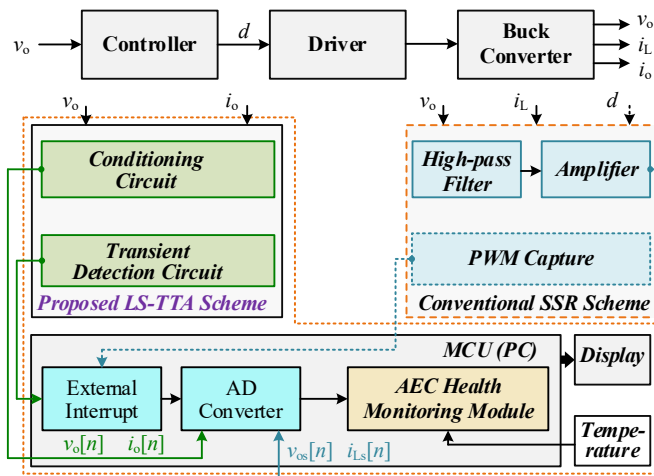


Fig. 1. Main circuit of a synchronous buck converter with an equivalent model of AEC.



LS-TTA large-signal transient trajectory analysis SSR steady-state ripple

Fig. 2. Block diagram of the SSR based monitoring scheme and the proposed LS-TTA scheme.

the series connection of a pure resistor  $R_C$  ( $ESR$ ) and a pure capacitor  $C$ .

Fig. 2 gives the block diagram of the proposed LS-TTA scheme, which consists of a signal conditioning circuit, a transient detection circuit and a microcontroller unit (MCU). The signal conditioning circuit is employed to adjust the voltage and current signals to make them adapt to the MCU. The transient detection circuit is designed to detect the large-signal load transient, so as to trigger the analog-to-digital (AD) converter to sample the transient voltage and current signals. Using the sampled transient voltage  $v_o[n]$  and current  $i_o[n]$ , the  $ESR$  and  $C$  are estimated, in order to realize the health state monitoring of AEC.

For comparison, Fig. 2 also shows the block diagram of the conventional steady-state ripple (SSR) based scheme. Different from the proposed scheme, the SSR scheme uses steady-state ripple signals to estimate the  $ESR$  and  $C$ . In the SSR scheme, the steady-state voltage and/or current ripples are obtained by a ripple extraction circuit consisting of a high-pass filter and an amplifier. Then using the MCU or PC to sample the ripple signals  $v_{os}[n]$ ,  $i_{Ls}[n]$  to compute the  $ESR$  and  $C$ . In [2], the pulse width modulation (PWM) signal is also needed as shown in the dotted line in Fig. 2.

Taking the unloading transient as an example, Fig. 3 (a) gives the steady-state and transient response waveforms of the output voltage  $v_o$  (indicated in red line), where the switching frequency  $f_s=200$  kHz.

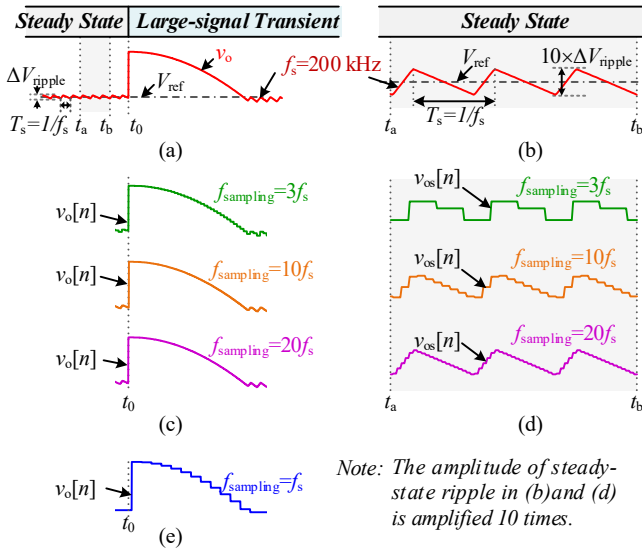


Fig. 3. Steady-state and unloading transient response waveforms of output voltage  $v_o$ . (a) Steady-state and unloading transient waveforms. (b) Steady-state waveforms under 10 times of magnification. (c) Transient sampling waveforms when  $f_{\text{sampling}} = 3f_s$ ,  $f_{\text{sampling}} = 10f_s$  and  $f_{\text{sampling}} = 20f_s$ . (d) Steady-state sampling waveforms when  $f_{\text{sampling}} = 3f_s$ ,  $f_{\text{sampling}} = 10f_s$  and  $f_{\text{sampling}} = 20f_s$ . (e) Transient sampling waveform when  $f_{\text{sampling}} = f_s$ .

Referring to Fig. 3(a), before the moment  $t_0$ , the converter works in steady state and  $v_o$  equals to the reference voltage  $V_{\text{ref}}$ . At  $t_0$ , a large-signal negative load current step occurs, the converter works in a transient. Compared with the high-frequency small-amplitude steady-state voltage ripple, the voltage signals  $v_o$  during transient has the characteristics of large amplitude and long time scale. Fig. 3(b) shows the detailed waveform of a steady-state ripple during  $t_a$  to  $t_b$ , whose amplitude  $\Delta V_{\text{ripple}}$  is amplified 10 times. To compare the differences between sampling transient trajectory and steady-state ripple, Fig. 3(c) and Fig. 3(d) give their sampling waveforms  $v_o[n]$  and  $v_{\text{os}}[n]$ , respectively. Here, three different sampling frequencies  $f_{\text{sampling}}$  are taken as examples, i.e.,  $f_{\text{sampling}} = 3f_s$ ,  $f_{\text{sampling}} = 10f_s$  and  $f_{\text{sampling}} = 20f_s$ . From Fig. 3 (c) and Fig. 3 (d), it is known that  $v_o[n]$  can represent the transient trajectory of  $v_o$  when using a relatively low sampling frequency (e.g.  $f_{\text{sampling}} = 3f_s$ ). However, the sampled signal  $v_{\text{os}}[n]$  can accurately represent the steady-state voltage ripple only under the case that  $f_{\text{sampling}} > 10f_s$ . From Fig. 3 (a), the transient trajectory is a long time-scale signal, whose period is larger than the switching cycle  $T_s$ . A lower sampling frequency (e.g.  $f_{\text{sampling}} = f_s$ ) satisfies the Nyquist rate [43]. Fig. 3 (e) gives the transient sampling waveform when  $f_{\text{sampling}} = f_s$ . It is illustrated that  $v_o[n]$  can represent the transient trajectory when  $f_{\text{sampling}} = f_s$ .

Based on the above analysis, it is found that sampling of the transient voltage trajectory does not require very high sampling frequency when compared with the sampling of steady-state ripple signals. Therefore, the main idea of the proposed scheme is to use the transient voltage trajectory to online estimate the AEC parameters to realize the health monitoring of AEC.

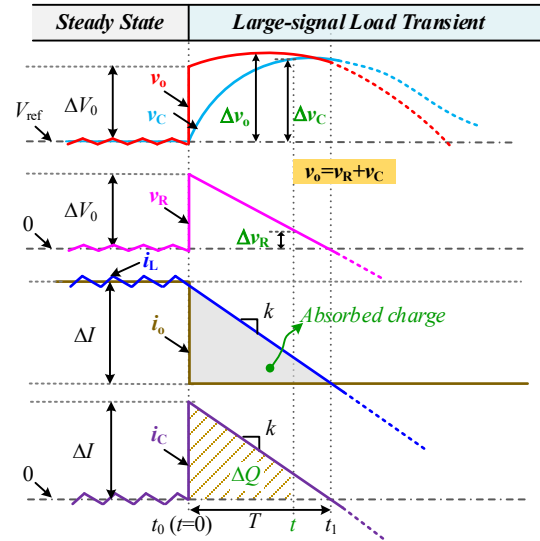


Fig. 4. Detailed unloading transient response waveforms for buck converter.

### III. CALCULATION MODEL AND SIMULATION VERIFICATION

#### A. Calculation model of ESR and C

Fig. 4 gives the detailed unloading transient response waveforms of output voltage  $v_o$ , pure capacitor voltage  $v_c$ , ESR voltage  $v_R$ , inductor current  $i_L$ , load current  $i_o$  and capacitor current  $i_c$ . At  $t_0$  ( $t=0$ ), a negative load current step  $\Delta I$  occurs, the capacitor absorbs the excess current, so as to cause the capacitor to charge and enable the capacitor voltage  $v_c$  increase [44]. At  $t_1$ ,  $i_L$  reaches the new load current, the capacitor stops charging and starts to discharge so as to cause  $v_c$  to decrease. Here, defining the charging period as  $T$ .

Assuming  $v_o$  is constant during  $t_0 \sim t_1$ , the inductor current slew rate is

$$k = |di_L/dt| = v_o/L. \quad (1)$$

At arbitrary moment  $t$ , the capacitor current  $i_c$  is calculated as

$$i_c(t) = \Delta I - kt. \quad (2)$$

The charge absorbed by the capacitor, i.e., the area of striped shadow region is calculated as

$$\Delta Q(t) = \int_0^t i_c(t) dt = \frac{1}{2} t (2\Delta I - kt). \quad (3)$$

From Fig. 1 and Fig. 4,  $v_o = v_c + v_R$ . Two factors determine the output voltage overshoot  $\Delta v_o$  during the charged interval  $t_0 \sim t_1$ : voltage overshoot  $\Delta v_R$  due to the ESR and voltage overshoot  $\Delta v_c$  due to charge of the capacitor, thus, we have

$$\begin{cases} v_o(t) = V_{\text{ref}} + \Delta v_o(t) \\ \Delta v_o(t) = \Delta v_c(t) + \Delta v_R(t) \\ \Delta v_c(t) = \Delta Q(t)/C \\ \Delta v_R(t) = R_C i_c(t) \end{cases} \quad (4)$$

Substituting (2), (3) into (4), the voltage overshoot  $\Delta v_o$  is calculated as

$$\Delta v_o(t) = \frac{\Delta I}{C} t - \frac{1}{2} \frac{k}{C} t^2 + \Delta I R_C - k R_C t. \quad (5)$$

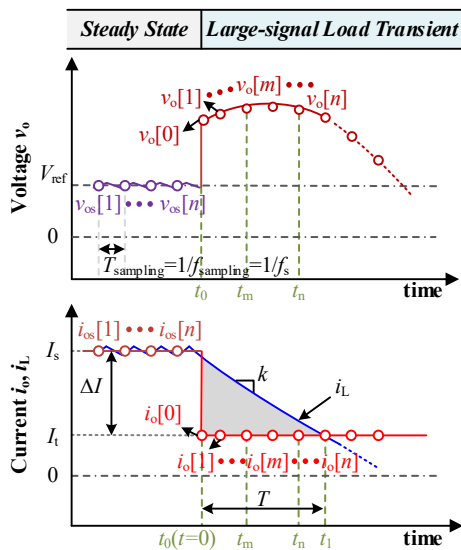


Fig. 5. Waveforms of sampling signal  $v_o[n]$ ,  $i_o[n]$  during an unloading transient.

Similarly, the voltage undershoot  $\Delta v'_o$  for a positive load step  $\Delta I$  is calculated as (6), where the inductor current slew rate  $k'=(v_i-v_o)/L$ .

$$\Delta v'_o(t) = \frac{\Delta I}{C}t - \frac{1}{2} \frac{k'}{C}t^2 + \Delta I R_C - k'R_C t. \quad (6)$$

At  $t=0$ , referring to Fig. 3, (5) and (6) are simplified as  $\Delta v_o(t=0)=\Delta v'_o(t=0)=\Delta I R_C$ , i.e.,

$$R_C = \frac{\Delta V'_o}{\Delta I} = \frac{\Delta V'_o}{\Delta I}. \quad (7)$$

Referring to the transient sampling waveforms in Fig. 5, equation (7) is written as (8), where  $f_{\text{sampling}}=f_s$  and  $v_{os}[n]$ ,  $i_{os}[n]$  are the steady-state sampling signals.

$$R_C = \frac{v_o[0] - v_o[n]}{i_o[0] - i_o[n]}. \quad (8)$$

In Fig. 5,  $v_o[m]$ ,  $i_o[m]$  and  $v_o[n]$ ,  $i_o[n]$  are the sampling signals at the sampling moments  $t_m$  and  $t_n$ . According to (5) and (6), the capacitance  $C$  is estimated as

$$C = \frac{2|i_o[0] - i_o[n]|(t_n - t_m) - k(t_n^2 - t_m^2)}{2[v_o[n] - v_o[m] + kR_C(t_n - t_m)]}. \quad (9)$$

For the actual system,  $v_o$  is not constant during transients. Hence, the inductor current slew rate  $k$  can be approximately calculated by the average value of  $v_o$ , i.e.,

$$k = \left( \sum_m^n v_o[n] \right) / (n - m + 1)L. \quad (10)$$

### B. Estimation error analysis

In the above analysis, we assume that  $v_o=V_{\text{ref}}$  when a load transient occurs (i.e., at  $t_0$ ). Considering the effect of steady-state ripple voltage  $\Delta V_{\text{ripple}}$ , Fig. 6 shows the unloading transient waveforms of output voltage and inductor current under two special cases. In Case I, the load transient occurs when  $v_o$  reaches the maximum value of the ripple voltage, i.e.,  $v_o=V_{\text{ref}}+\Delta V_{\text{ripple}}$ . In Case II, the transient occurs when  $v_o$  reaches the minimum value, i.e.,  $v_o=V_{\text{ref}}-\Delta V_{\text{ripple}}$ . According to (7),

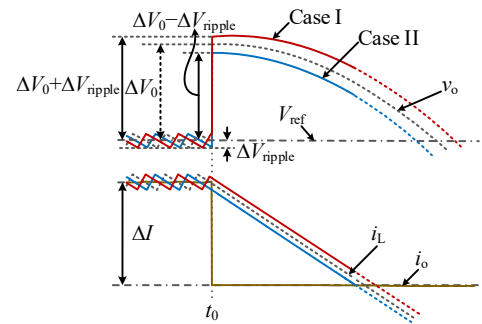


Fig. 6. Unloading transient waveforms of output voltage and inductor current when considering the effect of steady-state ripple voltage.

both of the two cases have the maximum estimation error  $\delta_{\text{max}}$  of  $ESR$ , which is calculated as

$$\delta_{\text{max}} = \Delta V_{\text{ripple}} / \Delta I. \quad (11)$$

From (11), it is known that  $\delta_{\text{max}}$  decreases as  $\Delta I$  increases, therefore, a large-signal load step is more suitable for parameters estimation. According to Fig. 5, in order to realize the capacitance estimation, the time intervals  $T$  at least 3 times the switching period  $T_s$ . Therefore, we define the large-signal load transient as  $T \geq 4T_s$ . From Fig. 4 and Fig. 5,  $T = \Delta I / k \approx (\Delta I \times L) / V_{\text{ref}}$ . Hence, the restrictive condition of estimation is calculated as

$$\Delta I \geq (4T_s v_o) / L \approx (4T_s V_{\text{ref}}) / L. \quad (12)$$

### C. Simulation verification

To verify the proposed  $ESR$  and  $C$  estimation method, synchronous buck converters with different capacitor parameters are built in the PSIM simulation environment. The main circuit parameters are given as follows:  $V_i=48$  V,  $V_o=12$  V,  $L=50$   $\mu\text{H}$ ,  $C=220$   $\mu\text{F}/100$   $\mu\text{F}$ ,  $f_s=200$  kHz. Analog proportional-integral (PI) controller is chosen as an example, the proportion coefficient  $k_p$  and integral constant  $\tau$  are 1.2 and 0.003 respectively. It is important to note that the  $C$  and  $ESR$  utilized in the simulation are assumed values, which are used to simulate the parameter change of capacitors.

According to the restrictive condition in (12),  $\Delta I$  should satisfy the relationship that  $\Delta I \geq 4.8$  A. Taking 5 A unloading transient as an example, Fig. 7 gives the simulation results, where Fig. 7(a) shows the results for  $C=220$   $\mu\text{F}$  and Fig. 7(b) shows that for  $C=100$   $\mu\text{F}$ . In the simulations, three different resistance values (50 m $\Omega$ , 100 m $\Omega$  and 150 m $\Omega$ ) are connected in series with capacitors to simulate the  $ESR$ , the corresponding output voltage and inductor current waveforms are shown in Fig. 7.

From Fig. 7, it is known that the transient voltage trajectory changes when the capacitor parameters are changed. The maximum voltage overshoot is determined by the capacitance when  $ESR$  is small, otherwise, it is determined by the  $ESR$ . According to the transient trajectory and (8)~(10), the estimated  $ESR$  and  $C$  are listed in Table I. The calculation results in Table I illustrate the feasibility of the proposed method. However, because of the effect of steady-state ripple voltage, the transient jump voltage  $\Delta V_0 = v_o[0] - V_{\text{ref}}$  has errors,

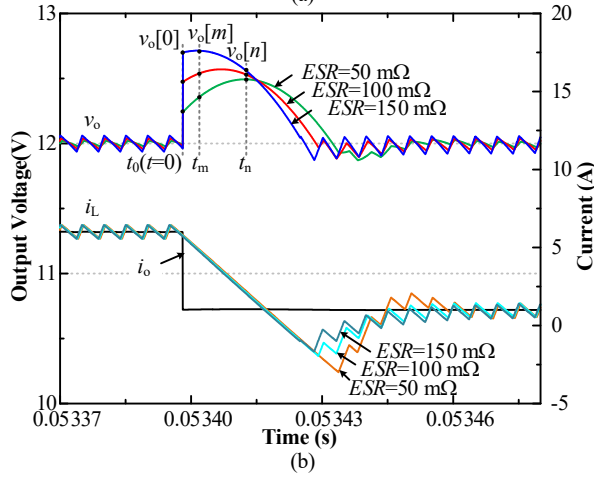
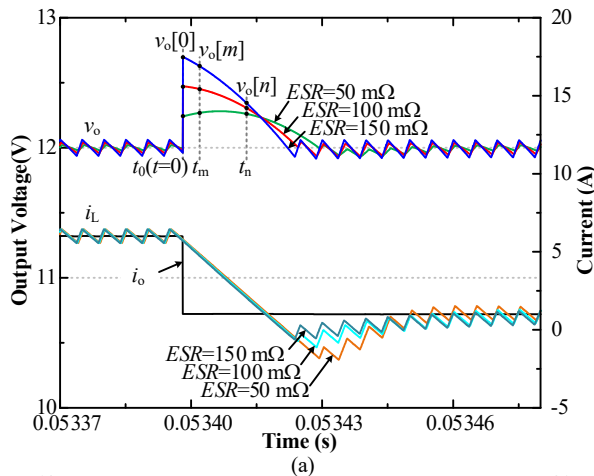


Fig. 7. Simulation results for the case that  $\Delta I$  is constant ( $\Delta I=5$  A). (a):  $C=220 \mu\text{F}$ ,  $ESR$  equals  $50 \text{ m}\Omega$ ,  $100 \text{ m}\Omega$  and  $150 \text{ m}\Omega$ . (b):  $C=100 \mu\text{F}$ ,  $ESR$  equals  $50 \text{ m}\Omega$ ,  $100 \text{ m}\Omega$  and  $150 \text{ m}\Omega$ .

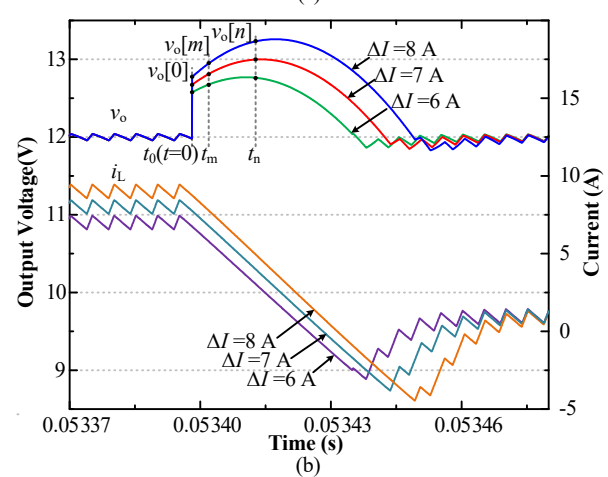
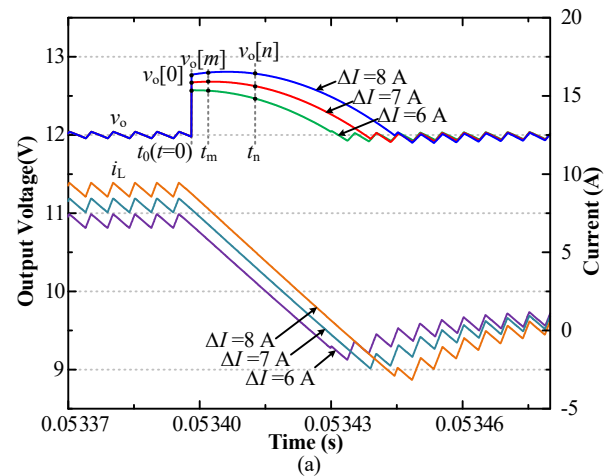


Fig. 8. Simulation results for the case that  $\Delta I$  equals to 6 A, 7 A, and 8 A. (a):  $C=220 \mu\text{F}$ ,  $ESR=100 \text{ m}\Omega$ . (b):  $C=100 \mu\text{F}$ ,  $ESR=100 \text{ m}\Omega$ .

TABLE I  
ESTIMATED RESULTS FOR THE CASE THAT  $\Delta I$  IS CONSTANT

Reference Values (Assumed Values)	Estimated $ESR$		Estimated $C$	
	Value( $\text{m}\Omega$ )	Error(%)	Value( $\mu\text{F}$ )	Error(%)
<b>220 <math>\mu\text{F}</math>, 50 <math>\text{m}\Omega</math></b>	48.4	3.2	210.1	4.5
<b>220 <math>\mu\text{F}</math>, 100 <math>\text{m}\Omega</math></b>	94.6	5.4	233.3	6
<b>220 <math>\mu\text{F}</math>, 150 <math>\text{m}\Omega</math></b>	139.7	6.8	237.3	7.8
<b>100 <math>\mu\text{F}</math>, 50 <math>\text{m}\Omega</math></b>	48.7	2.6	103.5	3.5
<b>100 <math>\mu\text{F}</math>, 100 <math>\text{m}\Omega</math></b>	95.1	4.9	105.6	5.6
<b>100 <math>\mu\text{F}</math>, 150 <math>\text{m}\Omega</math></b>	140.2	6.5	107.4	7.4

which leads to that the estimated  $ESR$  is inaccurate. The results demonstrate that the error of  $ESR$  is less 7% and the accuracy increases as the  $ESR$  decreases. In practice, we can use the average values of multiple estimated to define the  $ESR$ , in order to improve the accuracy. Moreover, from (9), it is known that the  $C$  is obtained using the estimated  $ESR$ , therefore, its error is relatively large.

In order to verify the ability of the proposed scheme to estimate  $ESR$  and  $C$  under different load steps, simulation results for different load steps ( $\Delta I$  equals to 6 A, 7 A and 8 A) are given in Fig. 8, where Fig. 8(a) shows the results when  $C=220 \mu\text{F}$ ,  $ESR=100 \text{ m}\Omega$  and Fig. 8(b) shows that for  $C=100 \mu\text{F}$ ,  $ESR=100 \text{ m}\Omega$ . According to the simulation waveforms, the calculation results are listed in Table II. The estimated results

TABLE II  
ESTIMATED RESULTS FOR THE CASE THAT  $ESR$  IS CONSTANT

Reference Values (Assumed Values)	Load Steps	Estimated $ESR$		Estimated $C$	
		Value ( $\text{m}\Omega$ )	Error (%)	Value ( $\mu\text{F}$ )	Error (%)
<b>220 <math>\mu\text{F}</math>, 100 <math>\text{m}\Omega</math></b>	6 A	96.4	3.6	232.4	5.6
	7 A	97.1	2.9	229.7	4.4
	8 A	97.6	2.4	227.5	3.4
<b>100 <math>\mu\text{F}</math>, 100 <math>\text{m}\Omega</math></b>	6 A	97	3	104.5	4.5
	7 A	97.9	2.1	102.9	2.9
	8 A	98.1	1.9	101.7	1.7

illustrate that the proposed method is feasible in the case of different load steps. The estimation errors decrease as  $\Delta I$  increases, and the error is relatively large when  $\Delta I$  is small.

Digital controlled buck converters are also widely used in modern engineering applications. Fig. 9 shows the simulation for digital PI controlled converter, where  $C=220 \mu\text{F}$ ,  $ESR=100 \text{ m}\Omega$ ,  $\Delta I=5$  A,  $k_p=0.6$ ,  $\tau=0.0015$ . Comparing with the analog controller, digital controller has a control delay  $t_{\text{delay}}$ . Here, the triangle-wave modulation is utilized and  $t_{\text{delay}} \approx 1.5 T_s$  [43]. To accurately estimate  $C$ , we set

$$t_m - t_0 \geq t_{\text{delay}}. \quad (13)$$

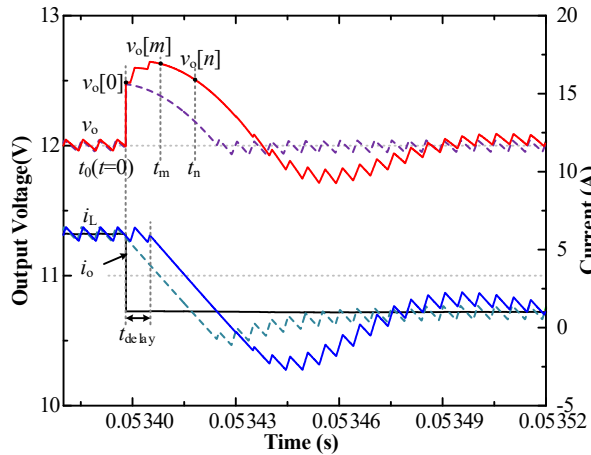


Fig. 9. Simulation results for digital controlled buck converter

TABLE III

ESTIMATED RESULTS FOR DIGITAL CONTROLLED BUCK CONVERTER

Reference Values (Assumed Values)	Estimated Value (mΩ)	Estimated Error (%)	Estimated Value (μF)	Estimated Error (%)
220 μF, 100 mΩ	97.6	2.4	238.4	8.3

Considering the control delay, (9) can be written as

$$C = \frac{2[i_o[0] - i_o[n]](t_n - t_m) - k[(t_n - t_{\text{delay}})^2 - (t_m - t_{\text{delay}})^2]}{2[v_o[n] - v_o[m] + kR_C(t_n - t_m)]} \quad (14)$$

According to the simulation waveforms, the calculation results are listed in Table III. The estimated results illustrate the proposed method is feasible for digital controlled converters.

#### IV. MONITORING SYSTEM DESIGN AND EXPERIMENTAL VERIFICATION

To verify the proposed AEC health online monitoring scheme, 48V-12V synchronous buck converters with digital PI controller and analog  $V^2$  controller are built and tested. The key parameters of the buck converters are given as follows:  $V_i=48$  V,  $V_o=12$  V,  $L=49.2$  μH,  $C=220$  μF/100 μF,  $f_s=200$  kHz. Three types of capacitors are selected for experimental verification, where the type of Capacitors I, II is Nichicon 220 μF/25 V (85 °C), the type of Capacitor III is Nichicon 100 μF/25 V (85 °C). The Capacitors I, III are new capacitors, and Capacitor II is a new capacitor connected in series with a resistor (used to simulate the parameters change).

##### A. Initial parameters acquirement

The proposed AEC health assessment scheme is based on the comparison of online estimated parameters and initial parameters. As reported in [45], the initial values  $ESR_0$ ,  $C_0$  of  $ESR$  and  $C$  change with the variation of ambient temperature  $Tem$ .  $ESR_0$  and  $C_0$  can be written as

$$\begin{cases} ESR_0(Tem) = \alpha + \beta e^{-Tem/\gamma} \\ C_0(Tem) = \chi + \lambda e^{-Tem/\nu} \end{cases} \quad (15)$$

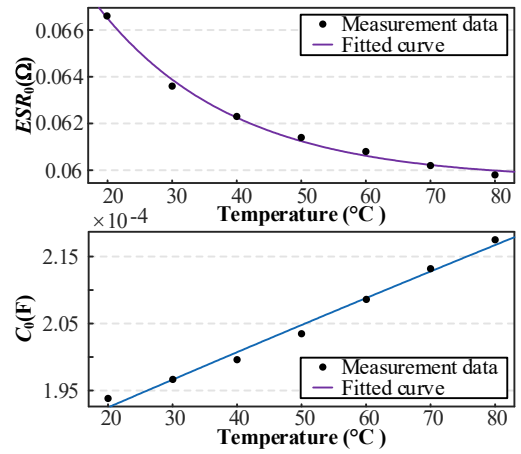


Fig. 10.  $ESR_0$  and  $C_0$  variation versus temperature of one capacitor (220 μF/25 V).

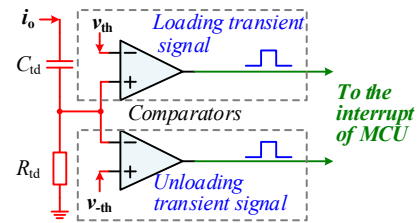


Fig. 11. Transient detection circuit.

TABLE IV

CHARACTERISTICS COEFFICIENTS OF  $ESR_0$  AND  $C_0$

Coefficients	Capacitor I (220 μF/25V)	Capacitor II (220 μF/25V)	Capacitor III (100 μF/25V)
$\alpha$ (Ω)	0.05959	0.1779	0.1246
$\beta$ (Ω)	0.01791	0.01791	0.03181
$\gamma$ (°C)	21	21	26
$\chi$ (F)	0.0006006	0.0006006	0.00002726
$\lambda$ (F)	-0.0004166	-0.0004166	-0.00001816
$\nu$ (°C)	980	980	880

where  $\alpha$ ,  $\beta$ ,  $\gamma$ ,  $\chi$ ,  $\lambda$ , and  $\nu$  are characteristics coefficients. To obtain these coefficients, the initial values at different operating temperatures are offline measured by using LCR meter (GW Instek LCR-8000G). Taking Capacitors I as an example, Fig. 10 shows the measurement results. Using curve fitting [23], [28], the values of these coefficients are listed in Table IV.

##### B. Transient detection circuit design

Referring to Fig. 11, an RC differential circuit consisting of  $C_{id}$  and  $R_{id}$  is used for the load transient detection, and comparator is employed for the threshold detection ( $v_{th}$  and  $v_{-th}$  is the threshold voltage). According to the detection principle discussed in [36], the parameters are designed as  $C_{id}=500$  pF,  $R_{id}=10$  kΩ.

##### C. Sampling moment selection

In the analysis of Section III, we ignore the equivalent series inductance ( $ESL$ ) of AEC. Considering the  $ESL$ , Fig. 12(a) gives the equivalent circuit. Under the effect of  $ESL$ , the output voltage jump  $\Delta V_o$  at the load step moment  $t_0$  consists of two parts, i.e., the voltage jump  $\Delta V_{R_0}$  caused by  $ESR$  and voltage jump  $\Delta V_{L_0}$  caused by  $ESL$ , as shown in Fig. 12(b).

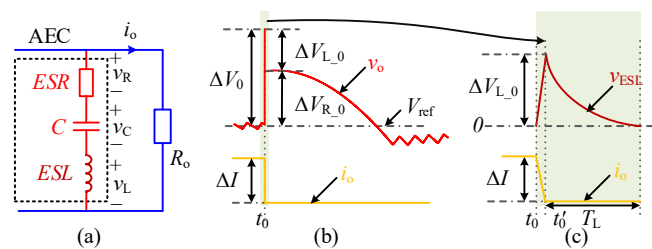


Fig. 12. The transient waveforms when considering the *ESL*. (a) Equivalent circuit. (b) Transient waveforms. (c) Detailed transient waveforms near the moment  $t_0$ .

From Fig. 12 (b), the voltage jump  $\Delta V_{L,0}$  is a short-time transient signal and it only occurs near the instant  $t_0$  (the shadow area). To calculate  $\Delta V_{L,0}$  and its attenuation time, Fig. 12 (c) gives the detailed waveforms of  $\Delta V_{L,0}$  and  $\Delta I$  near the moment  $t_0$ . At  $t_0$ , the load current starts to change, it reaches the new value at  $t_0'$ , and the time interval from  $t_0$  to  $t_0'$  is extremely short (close to 0). According to the circuit law [47],  $\Delta V_{L,0} = ESL \cdot di_o/dt$ . At  $t_0'$ , the energy stored in the *ESL* starts to release. Ignoring the effect of capacitor near  $t_0$ , the circuit is approximated as an *LR* resonance circuit. The attenuation time  $T_L$  is about as 4 time constant of, i.e.,

$$T_L \approx 4 \cdot ESL / (ESR + R_o). \quad (16)$$

For Capacitors I, II and III, the measured *ESL* is all about 10 nH. Using (16), for a 5 A load current, the values of  $T_L$  are about 0.02  $\mu$ s. To avoid the sampling of  $v_{ESL}$ , the sampling of  $v_o[0]$  should be after the moment that  $t_0 + T_L$ .

#### D. Experimental results

Fig. 13 shows the photo of the built experimental platform, where the Buck Converter I employs a digital PI controller, and Converter II utilizes the analog  $V^2$  control scheme. For Converter I, the MCU TMS320F28377D is used to implement the digital control algorithm as well as the online estimation of *ESR* and *C*, i.e., the equations (9) and (14). For Converter II, the MCU is only used for online monitoring of AEC. In experiments, all measurements and tests are done under room temperature (i.e.,  $T_{em} = 20$  °C). According to (15), the initial values of Capacitors I, II and III are listed in Table V.

The detailed AEC online monitoring flowchart is shown in Fig. 14, where the ambient temperature is measured using the internal temperature sensor in the MCU. When the load transient happens, the transient detection circuit generates a pulse signal to trigger the external interrupt of MCU and enables the ADC to sample the voltage and current signals at the transient initial moment (i.e.,  $t_0 + T_L$ ) to realize the calculation of *ESR*. Then the ADC starts to sample the transient voltage and current trajectories to calculate *C*. It is known that the capacitor aging is a slow process. There is no need to estimate capacitor parameters in real-time. Therefore, the online estimation is only taken when the load step satisfies the restrictive condition in (12). Referring to Fig. 14, to avoid the false triggering of external interrupt, the interrupt pin of MCU is set as input qualification mode [48]. Here, unwanted noises are eliminated by a sampling window, the width of the sampling window is defined as three system clock of MCU.

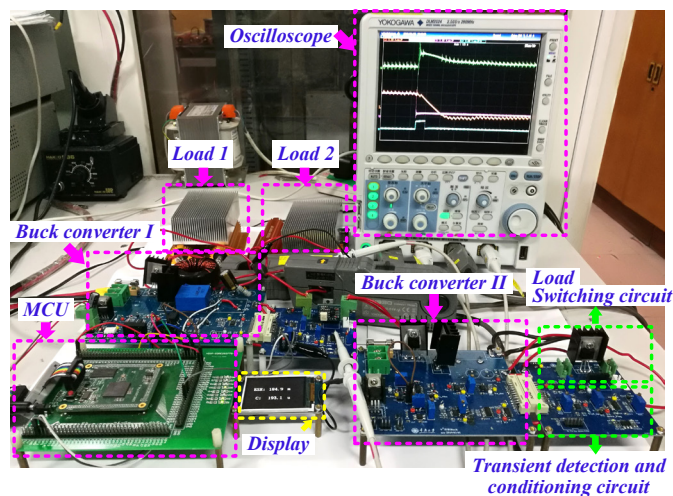


Fig. 13. Experimental platform with converters and loads.

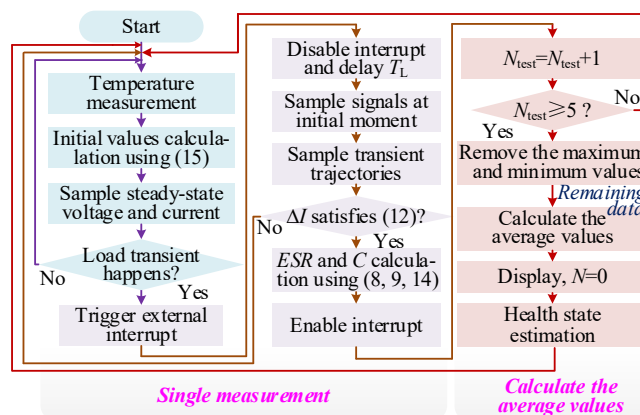


Fig. 14. Flowchart of the online monitoring system.

TABLE V  
INITIAL VALUES OF CAPACITORS I, II AND III WHEN  $T_{em} = 20$  °C

Capacitors	Tested initial values
Capacitor I: 220 $\mu$ F/25 V	66.6 m $\Omega$ , 193.8 $\mu$ F
Capacitor II: 220 $\mu$ F/25 V	184.9 m $\Omega$ , 193.8 $\mu$ F
Capacitor III: 100 $\mu$ F/25 V	139.8 m $\Omega$ , 95.6 $\mu$ F

Moreover, in order to ensure the sampling and calculation are not affected by other processes, such as the next load change, the external interrupt during the parameter estimation period is disabled. From the right part of Fig. 14, a median value filter and average algorithm are used to inhabit random error and improve the measurement accuracy. Actually, a whole process of parameter estimation is considerably short compared with the capacitor aging [32]. Therefore, the test times  $N_{test}$  can be set larger to obtain more accurate results.

1) *Case of digital PI controlled buck converter*: Fig. 15 gives the experimental results of the Converter I under different unloading transients (at 20 °C), where the PWM utilizes the triangle-wave modulation and  $t_{delay} \approx 1.5 T_s$ . The ADC resolution is 12 bits, the controller parameters are  $k_p = 0.35$ ,  $\tau = 0.0025$ . Fig. 15 (a)–(b) show the results when Capacitor I is used, Fig. 15 (c)–(d), and Fig. 15 (e)–(f) show that when Capacitor II and III are employed. In each sub-graph, the left part shows the experimental waveforms, including output

voltage  $v_o$ , inductor current  $i_L$ , output current  $i_o$  and the unloading transient detection signal  $v_T$ . The right part of each sub-graph gives the voltage and current data sampled by the MCU. Using the proposed monitoring method, the estimated  $ESR$  and  $C$  are listed in Table VI.

According to the experimental waveforms in Fig. 15, it is found that the duty cycle of the buck converter can reach 0% during unloading transients (the period from  $t_0$  to  $t_1$ ) when the designed controller parameters are ideal. To verify the feasibility of the proposed scheme under the case that the controller parameters are non-ideal (the duty cycle is approximately equal to 0.8 during  $t_0$  to  $t_1$ ), Fig. 16 gives the experimental results when Capacitor I is used and  $\Delta I=5.5$  A,  $k_p=0.25$ ,  $\tau=0.0025$ . It is found that the transient voltage trajectory is close to the ideal voltage trajectory. Using (14), the estimated  $C$  is  $211.6 \mu\text{F}$  and the error is less 10%, which validated that the capability of the proposed scheme.

2) Case of analog  $V^2$  controlled buck converter: To verify the feasibility of the proposed monitoring scheme for the converter controlled by different types of controllers. Fig. 17

TABLE VI  
ESTIMATED  $ESR$  AND  $C$  FOR CONVERTER I

Load steps	Capacitors	Estimated $ESR$		Estimated $C$	
		Value (m $\Omega$ )	Error (%)	Value ( $\mu\text{F}$ )	Error (%)
$\Delta I=5.5$ A (6.5 A $\rightarrow$ 1 A)	Capacitor I	71.1	6.7	210.1	8.4
	Capacitor II	198.6	7.4	212.4	9.6
	Capacitor III	149.3	6.8	102.8	7.5
$\Delta I=8.5$ A (9.5 A $\rightarrow$ 1 A)	Capacitor I	70.3	5.6	205.4	5.9
	Capacitor II	195.9	5.9	206.3	6.4
	Capacitor III	147.5	5.5	101.2	5.9

gives the experimental results of the buck converter using  $V^2$  controller, where the error amplifier parameters are  $k_p=0.1$ ,  $\tau=0.001$ . Here, Capacitor II is used and Fig. 17 (a), (b) show the results when  $\Delta I=5.5$  A and 8.5 A, respectively. Using the proposed method, the estimated  $ESR$  and  $C$  are as listed in Table VII.

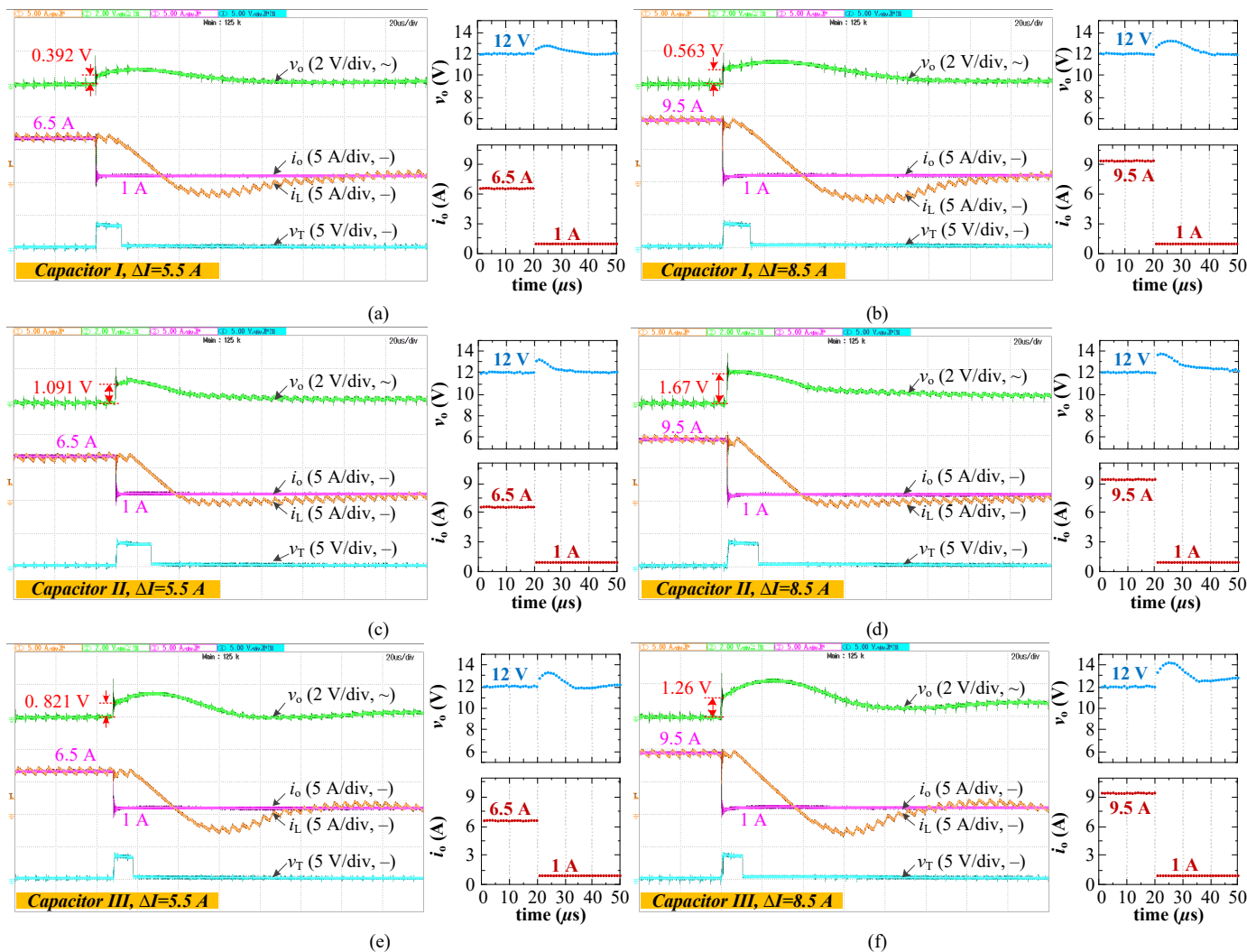


Fig. 15 Experimental results of the buck converter using a digital PI controller. (a) Using Capacitor I,  $\Delta I=5.5$  A. (b) Using Capacitor I,  $\Delta I=8.5$  A. (c) Using Capacitor II,  $\Delta I=5.5$  A. (d) Using Capacitor II,  $\Delta I=8.5$  A. (e) Using Capacitor III,  $\Delta I=5.5$  A. (f) Using Capacitor III,  $\Delta I=8.5$  A.

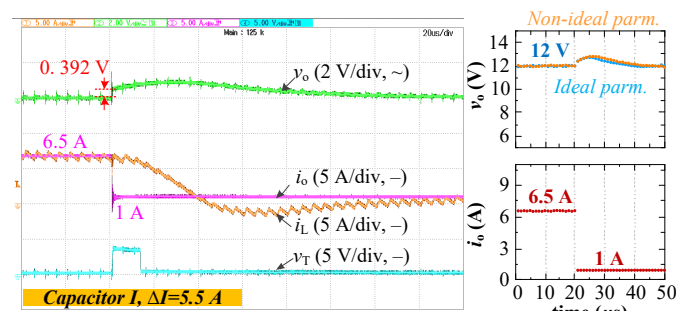


Fig. 16 Experimental results of the buck converter using a digital PI controller with non-ideal parameters.

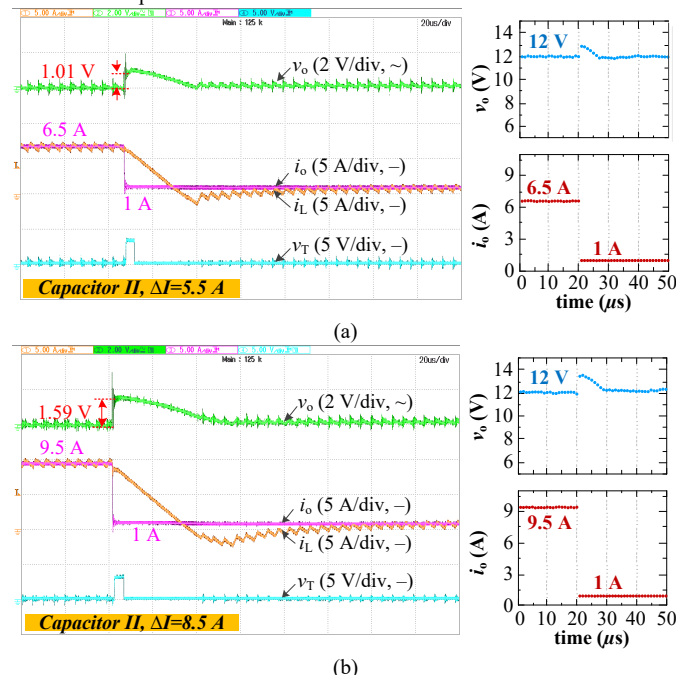


Fig. 17 Experimental results of the buck converter using an analog  $V^2$  controller. (a) Using Capacitor II,  $\Delta I=5.5$  A. (b) Using Capacitor II,  $\Delta I=8.5$  A.

TABLE VII  
ESTIMATED  $ESR$  AND  $C$  FOR CONVERTER II

Load steps	Capacitors	Estimated $ESR$		Estimated $C$	
		Value ( $m\Omega$ )	Error (%)	Value ( $\mu F$ )	Error (%)
$\Delta I=5.5$ A (6.5 A $\rightarrow$ 1 A)	Capacitor II	192.7	4.2	205.3	5.9
$\Delta I=8.5$ A (9.5 A $\rightarrow$ 1 A)	Capacitor II	189.6	2.5	198.9	2.6

From Tables VI and VII, it is demonstrated that the proposed  $ESR$  and  $C$  estimation method is feasible, and the estimation error is less than 10%. For comparison, Table VIII lists the existing  $ESR$  and/or  $C$  measurement methods for buck converters, where  $N$  is the number of sampling points during one switching cycle. The results illustrate that the proposed method is more suitable for high-frequency converters, compared to the SPI based methods. When comparing with the SSR and CM based methods, it is found that the number of sampling points is relatively low. However, the estimation error is relatively large, which is similar to that in [2]. It is the price of decreasing the sampling frequency.

#### E. Additional cost analysis

The proposed LS-TTA scheme induces extra hardware and software as with other capacitor monitoring schemes. To compare the extra cost, Table IX summarizes the additional hardware and software demand for capacitor monitoring in dc-dc converters. Here, the oscilloscope works as a signal sample device, which is used to sample and save high-frequency small-amplitude voltage and current signals. The PC works as a powerful signal processor to run complex identification algorithms.

TABLE VIII  
COMPARISON WITH THE EXISTING CAPACITOR MONITORING METHODS FOR BUCK CONVERTERS

Approach	Input/Output	Health Indicator	Description	$f_s$	$N$	Error
Offline method	N/A	$ESR, C$	[14]: Modulated sinusoidal waveforms are injected to the tested capacitor	N/A	N/A	Less than 16%
SPI based method	10V/3.3V	$ESR, C$	[19], [20], [21]: Small signal injection to obtain available signals, then using filter and optimization algorithm to calculate $ESR$ and $C$	20 kHz	1	Less than 1%
	48V/24V	$ESR$	[23]: Using circuits to extract the dc value of ripple voltage	50 kHz	N/A	N/A
SSR based method	10V/5V	$ESR$	[25]: Ripple current extraction using Rogowski Coil sensor	50 kHz, 100 kHz	Large than 100	Less than 5%
	12V/5V	$ESR$	[26]: Using the relationship between the slopes of the input current and of the output voltage	20 kHz	100	Less than 5%
	23V/10.7V	$ESR$	[27]: Empirical mode decomposition (EMD) algorithm on ripple voltage and inductor current	100 kHz	N/A	Less than 5%
	24V/12V	$ESR$	[29]: Wavelet transform denoising (WTD) algorithm on ripple voltage and inductor current	44.5 kHz	2247	Less than 1%
	13-120V/12V	$ESR, C$	[2]: Sampling voltage ripple at particular moments	10 kHz, 100 kHz	2	Less than 10%
CM based method	30V/15V	$ESR, C$	[33]: Hybrid model	20 kHz	150	Less than 7%
	12V/1.2-1.0.8V	$ESR, C$	[35]: Continuous time model	20 kHz	25	Less than 10%
	24V/5.3V	$C$	[38]: Adaptive model observes	300 kHz	666	Less than 5%
Proposed scheme	48V/12V	$ESR, C$	Load transient trajectory analysis	200 kHz	1	Less than 10%

TABLE IX  
ADDITIONAL HARDWARE AND SOFTWARE FOR CAPACITOR ONLINE MONITORING IN DC-DC CONVERTERS

Type	Method	Topology	Signal detection circuit/ device	Main component	additional	Data processing tool	Algorithm complexity	Ref.
I	SPI	Buck	Not required	Not required		MCU (also as a controller), PC, Matlab	+++	[19]–[21]
	SPI	Interleaved boost	Not required	Not required		FPGA, ARM (also as a controller), PC	+++	[22]
II	SSR	Non-isolated dc-dc	Ripple extraction circuit	Rogowski Coil sensor ( $\times 1$ )		PC, DS1104 board	+	[1], [25]
	SSR	Boost	Ripple extraction circuit, signal conditioning circuit	Amplifier ( $\times 1$ )		PCI card, PC with Matlab	+	[24]
	SSR	Buck	Oscilloscope	Not mentioned		PC with Matlab	+	[26]
	SSR	Boost	Oscilloscope	Tunnel magnetoresistance sensor ( $\times 2$ )		PC with Matlab	+	[28]
	SSR	Buck	Oscilloscope	Not mentioned		PC with Matlab	++	[29]
	SSR	Boost	Oscilloscope	Not mentioned		PC with Matlab	+	[30]
	CM	Buck, boost	Signal conditioning circuit	Hall sensor ( $\times 1$ ),		PC, PCI card, Matlab	++	[33]–[37]
	CM	Buck	Analog signal interface	Not mentioned		PC, dSPACE (also as a controller)	++	[38]
	CM	Boost	Oscilloscope	Not mentioned		PC with Matlab	++	[39]
III	SSR	Buck	PWM trigger circuit, ripple extraction circuit	Transformer ( $\times 2$ ), Amplifier ( $\times 4$ ), Comparator ( $\times 1$ ), D flip-flop ( $\times 2$ )		MCU	+	[2]
	SSR	Flyback	PWM trigger circuit, ripple extraction circuit	Transformer ( $\times 2$ ), Amplifier ( $\times 4$ ), Comparator ( $\times 2$ ), D flip-flop ( $\times 3$ )		MCU	+	[17], [32]
	SSR	Buck	DC voltage extraction circuit	Not mentioned		Not required (Unable to obtain parameter value)	+	[23]
	SSR	PV boost	Ripple extraction circuit	Comparator ( $\times 2$ )		MCU (also as a controller)	+	[31]
Proposed LS-TTA		Buck	Unloading transient detection circuit	Hall sensor ( $\times 1$ ), Comparator ( $\times 1$ )		MCU (also as a controller for digital control)	+	

TABLE X  
FEATURES OF DIFFERENT CATEGORIES IN TABLE IX [18]

Type	Description	Features
I	Software dependent	No additional hardware; High computational complexity, which limits the switching frequency. Expensive high-speed sampling devices, such as oscilloscope, data acquisition card, are needed;
II	Hardware dependent	Relatively low computational complexity, however, large amounts of data require to be processed by powerful software, such as MATLAB.
III	Economy	Sampling frequency and computational complexity are low, the condition monitoring can be taken using an MCU and low-cost signal processing circuits.

According to the dependence on software or hardware, these schemes can be divided into three categories. Table X shows the descriptions and main features of these categories. Referring to Table IX and Table X, the hardware and software demand of the proposed scheme is lower than that in Type I and Type II, which is similar to that in Type III. Moreover, compared to the schemes of Type III, the number of additional components in the proposed scheme is relatively low.

## V. CONCLUSION

In the paper, a transient trajectory analysis based scheme is proposed to online estimate the  $ESR$  and  $C$  of output capacitor for buck converters. Using the relationship between capacitor parameters and output voltage transient trajectory, the  $ESR$  and  $C$  are calculated. The main features of the proposed scheme are as follows: 1) Considering non-isolated buck converters often encounter step change in the load current, the  $ESR$  and  $C$  are estimated using transient trajectory. 2) Large-amplitude

transient voltage signals are utilized to estimate the capacitor parameters, without sampling high-frequency small-amplitude ripple signals. With the application of the proposed method to 48V-12V synchronous buck converters, experimental results demonstrate that the method is feasible.

## REFERENCES

- [1] H. Givi, E. Farjah and T. Ghanbari, "A Comprehensive Monitoring System for Online Fault Diagnosis and Aging Detection of Non-Isolated DC-DC Converters' Components," *IEEE Trans. Power Electron.*, vol. 34, no. 7, pp. 6858-6875, July 2019.
- [2] K. Yao, W. Tang, W. Hu, and J. Lyu, "A current-sensorless online  $ESR$  and  $C$  identification method for output capacitor of buck converter," *IEEE Trans. Power Electron.*, vol. 30, no. 12, pp. 6993-7005, Dec. 2015.
- [3] H. S.-H. Chung, H. Wang, F. Blaabjerg, and M. Pecht, *Reliability of Power Electronic Converter Systems*. London, U.K.: IET, 2015.
- [4] Y. Gupta, M. W. Ahmad, S. Narale and S. Anand, "Health Estimation of Individual Capacitors in a Bank With Reduced Sensor Requirements," *IEEE Trans. Ind. Electron.*, vol. 66, no. 9, pp. 7250-7259, Sept. 2019.
- [5] P. Sun, C. Gong, X. Du, Q. Luo, H. Wang, and L. Zhou, "Online condition monitoring for both IGBT module and DC-link capacitor of power

- converter based on short-circuit current simultaneously,” *IEEE Trans. Ind. Electron.*, vol. 64, no. 5, pp. 3662–3671, May 2017.
- [6] D. Zhou, Y. Song, Y. Liu and F. Blaabjerg, “Mission Profile Based Reliability Evaluation of Capacitor Banks in Wind Power Converters,” *IEEE Trans. Power Electron.*, vol. 34, no. 5, pp. 4665–4677, May 2019.
- [7] H. Wang, M. Liserre, and F. Blaabjerg, “Toward reliable power electronics: Challenges, design tools, and opportunities,” *IEEE Ind. Electron. Mag.*, vol. 7, no. 2, pp. 17–26, Jun. 2013.
- [8] S. Yang, D. Xiang, A. Bryant, P. Mawby, L. Ran, and P. Tavner, “Condition monitoring for device reliability in power electronic converters: a review,” *IEEE Trans. Power Electron.*, vol. 25, no. 11, pp. 2734–2752, Nov. 2010.
- [9] Y. T. Song and B. S. Wang, “Survey on reliability of power electronic systems,” *IEEE Trans. Power Electron.*, vol. 28, no. 1, pp. 591–604, Jan. 2013.
- [10] S. Yang, A. Bryant, P. Mawby, D. Xiang, L. Ran and P. Tavner, “An industry-based Survey of reliability in power electronic converters,” *IEEE Trans. on Ind. Appl.*, vol. 47, no. 3, pp. 1441–1451, May/June. 2011.
- [11] H. Soliman, H. Wang and F. Blaabjerg, “A review of the condition monitoring of capacitors in power electronic converters,” *IEEE Trans. on Ind. Appl.*, vol. 52, no. 6, pp. 4976–4989, Nov./Dec. 2016.
- [12] H. Nakao, Y. Yonezawa, T. Sugawara, Y. Nakashima, and F. Kurokawa, “Online evaluation method of electrolytic capacitor degradation for digitally controlled SMPS failure prediction,” *IEEE Trans. Power Electron.*, vol. 33, no. 3, pp. 2552–2558, Mar. 2018.
- [13] H. Wang and F. Blaabjerg, “Reliability of capacitors for dc-link applications in power electronic converters—An overview,” *IEEE Trans. Ind. Appl.*, vol. 50, no. 5, pp. 3569–3578, Sep./Oct. 2014.
- [14] A. M. R. Amaral and A. J. M. Cardoso, “A simple offline technique for evaluating the condition of aluminum electrolytic capacitors,” *IEEE Trans. Ind. Electron.*, vol. 56, no. 8, pp. 3230–3237, Aug. 2009.
- [15] A. M. R. Amaral and A. J. M. Cardoso, “Using Newton-Raphson method to estimate the condition of aluminum electrolytic capacitors,” in *Proc. IEEE Int. Symp. Ind. Electron.*, Jun. 2007, pp. 827–832.
- [16] A. Shrivastava, M. H. Azarian, C. Morillo. B. Sood and M. Pecht, “Detection and reliability risks of counterfeit electrolytic capacitors,” *IEEE Trans. Rel.*, vol. 63, no. 2, pp. 468–479, Jun. 2014.
- [17] K. Yao, C. Cao, and S. Yang, “Noninvasive online condition monitoring of output capacitor’s ESR and C for a flyback converter,” *IEEE Trans. Instrum. Meas.*, vol. 66, no. 12, pp. 3190–3199, Dec. 2017.
- [18] M. W. Ahmad, N. Agarwal, P. N. Kumar, and S. Anand, “Low-frequency impedance monitoring and corresponding failure criteria for aluminum electrolytic capacitors,” *IEEE Trans. Ind. Electron.*, vol. 64, no.7, pp. 5657–5666, Jul. 2017.
- [19] M. Algreer, M. Armstrong, and D. Giaouris, “Active online system identification of switch mode DC-DC power converter based on efficient recursive DCD-IIR adaptive filter,” *IEEE Trans. Power Electron.*, vol. 27, no.11, pp. 4425–4435, Nov. 2012.
- [20] X. Li and K. S. Low, “Low sampling rate online parameters monitoring of DC-DC converters for predictive maintenance using biogeography-based optimization,” *IEEE Trans. Power Electron.*, vol. 31, no. 4, pp. 2870–2879, Apr. 2016.
- [21] M. Ahmeid, M. Armstrong, S. Gadoue, M. Algreer, and P. Missailidis, “Real-time parameter estimation of DC-DC converters using a self-tuned Kalman filter,” *IEEE Trans. Power Electron.*, vol. 32, no. 7, pp. 5666–5674, Jul. 2017.
- [22] J. Poon, P. Jain, C. Spanos, S. K. Panda, and S. R. Sanders, “Fault prognosis for power electronics systems using adaptive parameter identification,” *IEEE Trans. Ind. Appl.*, vol. 53, no. 3, pp. 2862–2870, May/June. 2017.
- [23] Y.-M. Chen, H.-C. Wu, M.-W. Chou, and K.-Y. Lee, “Online failure prediction of the electrolytic capacitor for LC filter of switching-mode power converters,” *IEEE Trans. Ind. Electron.*, vol. 55, no. 1, pp. 400–406, Jan. 2008.
- [24] L. Ren, C. Gong and Y. Zhao, “An Online ESR Estimation Method for Output Capacitor of Boost Converter,” *IEEE Trans. Power Electron.*, vol. 34, no. 10, pp. 10153–10165, Oct. 2019.
- [25] E. Farjah, H. Givi, and T. Ghanbari, “Application of an efficient Rogowski coil sensor for switch fault diagnosis and capacitor ESR monitoring in non-isolated single switch DC-DC converters,” *IEEE Trans. Power Electron.*, vol. 32, no. 2, pp. 1442–1456, Feb. 2017.
- [26] A. M. R. Amaral and A. J. M. Cardoso, “On-line fault detection of aluminium electrolytic capacitors, in step-down DC-DC converters, using input current and output voltage ripple,” *IET Power Electron.*, vol. 5, no. 3, pp. 315–322, Mar. 2012.
- [27] G. H. Wang, Y. Guan, J. Zhang, L. F. Wu, and X. Y. Zheng, “ESR estimation method for DC-DC converters based on improved EMD algorithm,” in *Proc. IEEE Conf. Prognostics Syst. Health Manage*, May 2012, pp. 1–6.
- [28] W. Miao, X. Liu, K. H. Lam and P. W. T. Pong, “Condition Monitoring of Electrolytic Capacitors in Boost Converters by Magnetic Sensors,” *IEEE Sensors J.*, vol. 19, no. 22, pp. 10393–10402, 15 Nov.15, 2019.
- [29] L. Ren and C. Gong, “Online estimation scheme of output capacitor’s ESR and tan $\delta$  for Buck converter,” *IET Power Electron.*, vol. 12, no. 11, pp. 2978–2986, 18 9 2019.
- [30] G. M. Buiatti, J. A. Mart’in-Ramos, C. H. R. Garcia, and A. M. R. Amaral, “An online and noninvasive technique for the condition monitoring of capacitors in boost converters,” *IEEE Trans. Instrum. Meas.*, vol. 59, no. 8, pp. 2134–2143, Aug. 2011.
- [31] M. W. Ahmad, N. Agarwal and S. Anand, “Online monitoring technique for aluminum electrolytic capacitor in solar PV-based DC system,” *IEEE Trans. Ind. Electron.*, vol. 63, no. 11, pp. 7059–7066, Nov. 2016.
- [32] K. Yao, H. Li, L. Li, C. Guan, L. Li, Z. Zhang, J. Chen, “A Noninvasive Online Monitoring Method of Output Capacitor’s C and ESR for DCM Flyback Converter,” *IEEE Trans. Power Electron.*, vol. 34, no. 6, pp. 5748–5763, June 2019.
- [33] H. Ma, X. Mao, N. Zhang, and D. Xu, “Parameter identification of power electronic circuits based on hybrid model,” in *Proc. IEEE Power Electron. Spec. Conf.*, Jun. 12–16, 2005, pp. 2855–2860.
- [34] H. Ma and L. G. Wang, “Fault diagnosis and failure prediction of aluminum electrolytic capacitor in power electronic converters,” in *Proc. IEEE Ind. Electron. Conf.*, 2005, pp. 842–847.
- [35] G. M. Buiatti, A. M. R. Amaral, and A. J. Marques Cardoso, “A unified method for estimating the parameters of non-isolated DC/DC converters using continuous time models,” in *Proc. 29th Int. Telecommun. Energy Conf.*, 2007, pp. 334–341.
- [36] G. M. Buiatti, A. M. R. Amaral, and A. J. M. Cardoso, “An online technique for estimating the parameters of passive components in nonisolated DC/DC converters,” in *Proc. IEEE Int. Symp. Ind. Electron.*, 2007, pp. 606–610.
- [37] G. Buiatti, A. Amaral, and A. Cardoso, “ESR estimation method for dc/dc converters through simplified regression models,” in *Proc. Conf. Record IEEE 42nd Ind. Appl. Conf.*, Sep. 2007, pp. 2289–2294.
- [38] Z. Cen and P. Stewart, “Condition parameter estimation for photovoltaic buck converters based on adaptive model observers,” *IEEE Trans. Rel.*, vol. 66, no. 1, pp. 148–160, Mar. 2017.
- [39] L. Ren and C. Gong, “Modified hybrid model of boost converters for parameter identification of passive components,” *IET Power Electron.*, vol. 11, no. 4, pp. 764–771, 10 4 2018.
- [40] H. Nakao, Y. Yonezawa, T. Sugawara, Y. Nakashima, and F. Kurokawa, “Online evaluation method of electrolytic capacitor degradation for digitally controlled SMPS failure prediction,” *IEEE Trans. Power Electron.*, vol. 33, no. 3, pp. 2552–2558, Mar. 2018.
- [41] J. Hannonen, J. Honkanen, J. P. Strom, T. Karkkainen, S. Raisanen and P. Silventoinen, “Capacitor aging detection in a DC-DC converter output stage,” *IEEE Trans. Ind. Appl.*, vol. 52, no. 4, pp. 3224–3233, Jul./Aug. 2016.
- [42] Z. Shan, S. C. Tan, and C. K. Tse, “Transient mitigation of dc-dc converters for high output current slew rate applications,” *IEEE Trans. Power Electron.*, vol. 28, no. 5, pp. 2377–2388, May. 2013.
- [43] C. Luca, M. Dragan, M. Paolo, Z. Regan, *Digital Control of High-Frequency Switched-Mode Power Converters.*, New York, NY, USA: Wiley, 2015.
- [44] R. Singh and A. Khambadkone, “A buck derived topology with improved step-down transient performance,” *IEEE Trans. Power Electron.*, vol. 23, no. 6, pp. 2855–2866, Nov. 2008.
- [45] K. Abdennadher, P. Venet, G. Rojat, J.-M. Retif, and C. Rosset, “A real-time predictive-maintenance system of aluminum electrolytic capacitors used in uninterrupted power supplies,” *IEEE Trans. Ind. Appl.*, vol. 46, no. 4, pp. 1644–1652, Jul./Aug. 2010.
- [46] Z. Zhao, W. G. Lu, W. Chen, X. Du and H. H. lu, “Multi-Period Frame Transient Switching Control for Low-Voltage High-Current Buck Converter with a Controlled Coupled Inductor,” *IEEE Trans. Power Electron.*, vol. 34, no. 10, pp. 9743–9757, Oct. 2019.
- [47] J. W. Nilsson and S. Riedel, *Electric Circuits*, 9th ed. Englewood Cliffs, NJ, USA: Prentice-Hall, 2011.

[48] TMS320F2837xD *Dual-Core Microcontrollers Technical Reference Manual*, Texas Instruments, Texas, US. [Online]. Available:

<http://www.ti.com/cn/lit/ug/spruhm8i/spruhm8i.pdf>



**Zhaoyang Zhao** received the B.S. and M.S. degrees in electrical engineering from Northeast Agricultural University, Harbin, China, in 2014 and 2017, respectively. He is currently working toward the Ph.D. degree in electrical engineering in the School of Electrical Engineering, Chongqing University, Chongqing, China.

His research interests include condition monitoring and control of power electronic converters.



**Weiguo Lu** (M'14) received the B.S., M.S., and Ph.D. degrees in electrical engineering from Chongqing University, Chongqing, China, in 2000, 2003, and 2008, respectively.

He is currently a Professor in the School of Electrical Engineering, Chongqing University, Chongqing. He is the author or coauthor of more than 20 papers in journal or conference proceedings. His current research interests include the stability analysis and control strategies of switching power converters, and magnetic-resonance wireless power

transfer.



**Pooya Davari** (S'11–M'13–SM'19) received the B.Sc. and M.Sc. degrees in electronic engineering in 2004 and 2008, respectively, and the Ph.D. degree in power electronics from QUT, Australia, in 2013. From 2005 to 2010, he was involved in several electronics and power electronics projects as a Development Engineer. From 2013 to 2014, he was with QUT, as a Lecturer. He joined Aalborg University, in 2014, as a Postdoc, where he is currently an Associate Professor. He has been focusing on EMI, power quality and harmonic

mitigation analysis and control in power electronic systems. He has published more than 100 technical papers. He is the recipient of a research grant from the Danish Council of Independent Research (DFF-FTP) in 2016. Dr. Davari served as a Guest Associate Editor of IET journal of Power Electronics, IEEE Access Journal, Journal of Electronics and Journal of Applied Sciences. He is an Associate Editor of Journal of Power Electronics, Associate Editor of IET Electronics, Editorial board member of EPE journal and Journal of Applied Sciences. He is member of the International Scientific Committee (ISC) of EPE (ECCE Europe). Currently, he is a member of Joint Working Group six and Working Group eight at the IEC standardization TC77A.



**Xiong Du** (M'13) obtained his B.S., M.S., and Ph. D. degrees from Chongqing University, China in 2000, 2002, and 2005 respectively, all in the Electrical Engineering.

He has been with Chongqing University since 2002 and is currently a full professor in the School of Electrical Engineering, Chongqing University. He was a visiting scholar at Rensselaer Polytechnic Institute, Troy, NY from July 2007 to July 2008.

His research interests include power electronics

system reliability and stability. He is a recipient of the National Excellent Doctoral Dissertation of P.R. China in 2008.



**Herbert Ho-Ching Iu** (S'98–M'00–SM'06) received the B.Eng. (Hons) degree in electrical and electronic engineering from the University of Hong Kong, Hong Kong, in 1997. He received the Ph.D. degree in Electronic and Information Engineering from the Hong Kong Polytechnic University, Hong Kong, in 2000.

In 2002, he joined the School of Electrical, Electronic and Computer Engineering, the University of Western Australia where he is currently a Professor. His research interests include power electronics, renewable energy, nonlinear dynamics, current sensing techniques, and memristive systems.

Prof. Iu currently serves as an Associate Editor of IEEE Transactions on Power Electronics, IEEE Transactions on Smart Grids, IEEE Transactions on Network Science and Engineering, IEEE Transactions on Circuits and Systems--II and IEEE Access.



**Frede Blaabjerg** (S'86–M'88–SM'97–F'03) was with ABB-Scandia, Randers, Denmark, from 1987 to 1988. From 1988 to 1992, he got the PhD degree in Electrical Engineering at Aalborg University in 1995. He became an Assistant Professor in 1992, an Associate Professor in 1996, and a Full Professor of power electronics and drives in 1998. From 2017 he became a Villum Investigator. He is honoris causa at University Politehnica Timisoara (UPT), Romania and Tallinn Technical University (TTU) in Estonia.

His current research interests include power electronics and its applications such as in wind turbines, PV systems, reliability, harmonics, and adjustable speed drives. He has published more than 600 journal papers in the fields of power electronics and its applications. He is the co-author of four monographs and editor of ten books in power electronics and its applications. He has received 30 IEEE Prize Paper Awards, the IEEE PELS Distinguished Service Award in 2009, the EPE-PEMC Council Award in 2010, the IEEE William E. Newell Power Electronics Award 2014 and the Villum Kann Rasmussen Research Award 2014. He was the Editor-in-Chief of the IEEE TRANSACTIONS ON POWER ELECTRONICS from 2006 to 2012. He has been Distinguished Lecturer for the IEEE Power Electronics Society from 2005 to 2007 and for the IEEE Industry Applications Society from 2010 to 2011 as well as 2017 to 2018. In 2019-2020 he serves a President of IEEE Power Electronics Society. He is Vice-President of the Danish Academy of Technical Sciences too. He is nominated in 2014-2018 by Thomson Reuters to be between the most 250 cited researchers in Engineering in the world.